6th International Conference on Advances in Experimental Structural Engineering
11th International Workshop on Advanced Smart Materials and Smart Structures Technology
August 1-2, 2015, University of Illinois, Urbana-Champaign, United States

FBG-based Tendon Force Monitoring and Temperature Effect Estimation in Prestressed Concrete Girder

T.C. Huynh[1], T.C. Nguyen[2], T.H. Kim[3], and J.T. Kim[4]

1, *PhD Student, Smart Structures Engineering Laboratory, Pukyong National University, Busan, Korea.*
E-mail: ce.huynh@gmail.com.
2, *MS Student, Smart Structures Engineering Laboratory, Pukyong National University, Busan, Korea.*
E-mail: isca88@gmail.com.
3, *MS Student, Smart Structures Engineering Laboratory, Pukyong National University, Busan, Korea.*
E-mail: whrxkaos@naver.com.
4, *Professor, Smart Structures Engineering Laboratory, Pukyong National University, Busan, Korea.*
E-mail: idis@pknu.ac.kr.

ABSTRACT
This paper has been motivated to monitor the prestress force in prestressed concrete (PSC) girders and to estimate the effect of temperature on the variation of prestress forces. Firstly, a fiber optical sensor (FOS)-based prestress force monitoring method is proposed for unbonded tendons of PSC girders. A temperature-effect estimation model is presented to theoretically estimate the change of prestress force due to the temperature variation. Secondly, lab-scale experiments are performed on a PSC girder with a fiber Bragg grating (FBG)-sensor embedded smart tendon. A series of temperature variation and prestress-loss events are simulated for the PSC girder. Thirdly, the feasibility of the FOS-based prestress force monitoring method is experimentally verified for the prestress-loss cases under the constant temperature. Finally, the effect of temperature variation on the prestress force is estimated by the FBG-sensor embedded tendon and the temperature-effect estimation model.

KEYWORDS: *Prestressed concrete girder, unbonded tendon, prestress force, temperature effect, FBG sensor*

1. INTRODUCTION

For a variety of civil infrastructures, prestressed concrete (PSC) girders are major components to resist against loadings. The tendon force of PSC girders is the key parameter that should be appropriately monitored for its serviceability and safety against external loadings. For the past decades, many researchers have focused the possibility of utilizing global vibration characteristics of a structure as an indication of its structural damage (Adams et al. 1978; Stubbs and Osegueda 1990). Recently, research efforts have been made to investigate the relationship between the prestress-loss and the change in the dynamic behaviors of prestressed structures (Saiidi et al. 1994, Miyamoto et al. 2000). However, the so-called 'global vibration-based method' can characterize the overall structural integrity but the global approach is unable to locally identify the small size of prestress-loss.

Various research efforts have been made to monitor the prestress forces from direct measurements of tendon's strain (e.g., Tensmeg tension measuring gauges, electrical strain gauges and vibrating wires). For the real-time monitoring, however, those sensor types may suffer long-term risks and electrical noises. In the recent years, Fiber Optic Sensors (FOS) have been proved to be reliable for long-term measurement of various practical sensing works. Particularly, Fiber Bragg Grating (FBG) sensors show good performance for monitoring civil infrastructures due to their inherent self-referencing capability, light weight, and immunity to electromagnetic interference and corrosion. By adopting these advantages, Kim et al. (2011) developed a so-called 'smart tendon' by embedding an optical fiber sensor (FOS) into the steel core wire of a 7-wire prestressing tendon to measure its tensile strain. By employing the smart tendon, the prestress force could be monitored easily and directly from prestressed structures in the field. However, this fact also leads to an important issue that needs to be solved before real ambient applications. That is the performance of the FBG-sensor embedded smart tendon under the temperature variation since the FBG sensor itself is temperature-dependent. In the real-life conditions of prestressed structures, the temperature effects are believed to play an important role in the variation of the measured prestress forces beside structural damages due to the difference in the thermal expansion characteristics of structural components. Researchers have examined the thermal effects on the prestress force of cable-supported structures (Ni et al. 2005, Hong et al. 2009). For the PSC girders embedded with smart tendons, the change of tendon force due to the temperature variation should be evaluated to achieve robust prestress-loss

monitoring results. Furthermore, this could provide information about thermal behaviors of smart tendons in the field. This study has been motivated to monitor the prestress force in prestressed concrete (PSC) girders and to estimate the effect of temperature on the variation of prestress forces by the FBG-sensor embedded tendon.

2. THEORIES OF PRESTRESS FORCE MONITORING AND TEMPERATURE-EFFECT ESTIMATION

2.1. FOS-based Prestress Force Monitoring Method

A FOS-based prestress force monitoring method is proposed for unbonded tendons of PSC girders. The concept of fiber Bragg grating (FBG) strain sensor is illustrated in Figure 2.1(a). When a light source travels into the optical fiber, the Bragg grating reflects particular wavelengths of incident lights. The center wavelength of the reflected light, λ_B, varies with the optical fiber's refractive index, n_{eff}, and the Bragg grating spacing, Λ, according to the Bragg's law:

$$\lambda_B = 2n_{eff}\Lambda \tag{2.1}$$

The temperature variation ΔT and the mechanical strain of the FBG sensor ε independently affect on the refractive index of the optical fiber and the Bragg grating spacing resulting in the shift in the reflected wavelength, $\Delta\lambda B$, as follows (Othonos and Kalli 1999):

$$\frac{\Delta\lambda_B}{\lambda_B} = (1-P_e)\varepsilon + (\alpha+\xi)\Delta T \tag{2.2}$$

in which P_e is the effective strain-optic constant, and α and ξ are respectively the thermal expansion coefficient of the fiber and the thermo-optic coefficient. Note that P_e, α, and ξ are approximately 0.22, 0.55×10^{-6}, and 8.6×10^{-6} for silica, respectively (Kim et al. 2011). It is also noted that the first term of Eq. (2.2) completely results from mechanical actions on the FBG sensor while the second term is caused by thermal strain and thermal-optical effect of the optical fiber material itself.

Under the condition of temperature variation, however, the heat expansion of the host structure acts mechanically as an external load on the FBG sensor. Accordingly, once temperature change ΔT is measured, the thermal strain of the host structure can be determined from Eq. (2.2). Figure 2.1(b) schematizes a PSC girder with an unbonded tendon. A FBG-sensor is embedded into the core of the tendon to measure the tendon's strain. Once the FBG strain ε of the tendon is measured, the prestress force F can be estimated:

$$F = \varepsilon(E_T A_T) \tag{2.3}$$

in which $E_T A_T$ is the axial rigidity of the unbonded tendon.

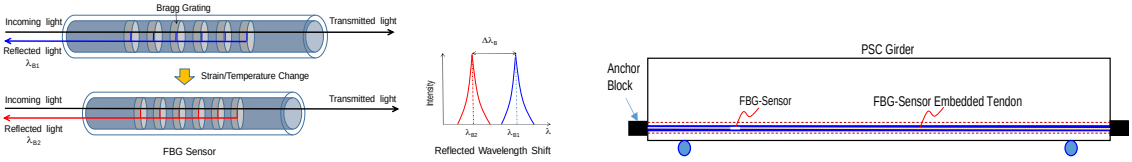

(a) Concept of FBG strain sensor (b) PSC girder with FBG-sensor embedded tendon

Figure 2.1 FOS-based prestress force monitoring in PSC girder

2.2. Temperature-Effect Estimation Model

For PSC girders, the variation of temperature affects the prestress force since the tendons length is fixed after the prestressing process, and the thermal expansion characteristics of steel and concrete are different. Once the thermal strain ε is measured, the tension force change ΔF could be estimated from its axial rigidity, $E_T A_T$, as:

$$\Delta F = -E_T A_T \varepsilon^T \tag{2.4}$$

Assume that the temperature distribution is uniform in the concrete girder and the embedded tendon. In order to prevent elongation, the anchors exert an equal and opposite tendon force ΔF on the tendon following a temperature change ΔT, as shown in Figure 2.2. In the elastic range, the elongation Δ_{PSC} of the PSC girder due to the temperature change ΔT can be estimated by:

$$\Delta_{PSC} = -\frac{\Delta F}{k_{PSC}} + \alpha_{PSC} L_{PSC} \Delta T \tag{2.5}$$

in which k_{PSC}, L_{PSC} and Δ_{PSC} are the compressive stiffness, the length, and the thermal expansion coefficient of the PSC girder, respectively.

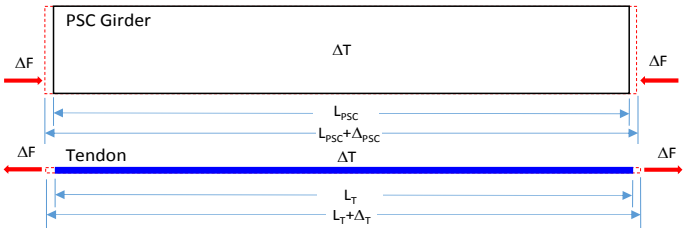

Figure 2.2 Equilibrium condition of PSC girder under thermal effect

For the elastic PSC girder subjected to an eccentric prestress force, the compressive stiffness corresponding to the eccentricity can be calculated by:

$$k_{PSC} = \frac{E_{PSC} A_{PSC}}{L_{PSC}} \frac{1}{\left(\frac{d^2 A_{PSC}}{I_{PSC}} + 1 \right)} \tag{2.6}$$

where E_{PSC} and A_{PSC} and I_{PSC} are, respectively, the elastic modulus, the cross-section area, and the moment of inertia of the PSC girder; and d signifies the eccentricity of the prestress force. On the other hand, the elastic elongation of the unbonded tendon ΔT can be expressed in term of temperature change ΔT, as follows:

$$\Delta_T = \frac{\Delta F}{k_T} + \alpha_T L_T \Delta T \tag{2.7}$$

in which L_T and ΔT are respectively the length and the thermal expansion coefficient of the unbonded tendon; and $k_T = E_T A_T / L_T$ is the corresponding tensile stiffness.
To meet the compatibility condition, the elongation of PSC girder is set equal to the elongation of the tendon as:

$$\Delta_{PSC} = \Delta_T \tag{2.8}$$

On substituting Eq. (2.5) and Eq. (2.7) into Eq. (2.8), by rearranging, the tendon force change is simplified as a function of the temperature variation as:

$$\Delta F = -kc\Delta T \tag{2.9}$$

in which c and k are defined as the longitudinal deformation per Celsius (m/°C) and the equivalent stiffness k (N/m) as follows:

$$c = (\alpha_T - \alpha_{PSC}) L \tag{2.10}$$

$$\frac{1}{k} = \left(\frac{1}{k_{PSC}} + \frac{1}{k_T} \right) \tag{2.11}$$

It is noted from Eq. (2.10) that $L_T = L_{PSC} = L$. Eq. (2.11) shows that the equivalent stiffness k is always a positive value. Therefore, the changing tendency of tendon force due to the temperature variation according to Eq. (2.9)

depends on the value of c which represents differences in thermal expansion coefficients between the unbonded tendon and the PSC girder, as revealed in Eq. (2.10). Once thermal expansion coefficients of PSC girders and unbonded tendons are specified, the temperature effect on the prestress force of PSC girders can be easily predicted by Eq. (2.9).

3. EXPERIMENTS ON PSC GIRDER WITH FOS-BASED SMART TENDON

3.1. FOS-based Smart Tendon

A FOS-based smart tendon is designed for prestress force monitoring in PSC girders. Figure 3.1(a) illustrates the concept of 7-wire smart tendon. Six outer steel wires are twisted around a carbon core wire in which an optical fiber with FBG-sensor is encapsulated. Diameters of the carbon core wire and the steel wire are 5.2 mm and 5.0 mm, respectively. For a lab-scale PSC girder tested in this study, a prestressing tendon embedded with three FBG strain sensors: FBG 1 (1520 nm), FBG 2 (1540 nm), and FBG 3 (1560 nm) as shown in Figure 3.1(b). Since the FBG strain sensors tightly embedded into the smart tendon, it could deform with the tendon under prestressing events.

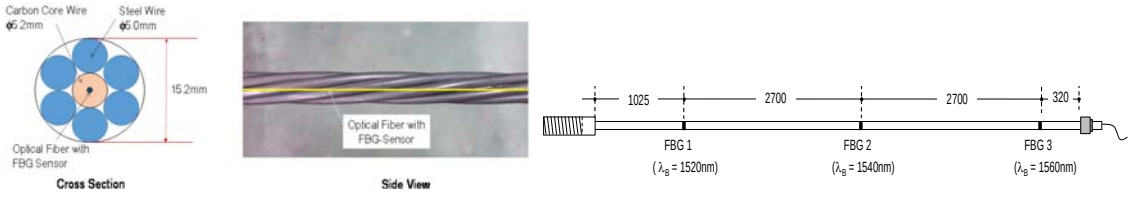

(a) Concept of smart tendon (b) Smart tendon embedded with 3 FBG sensors

Figure 3.1 Design of smart tendon for lab-scale PSC girder

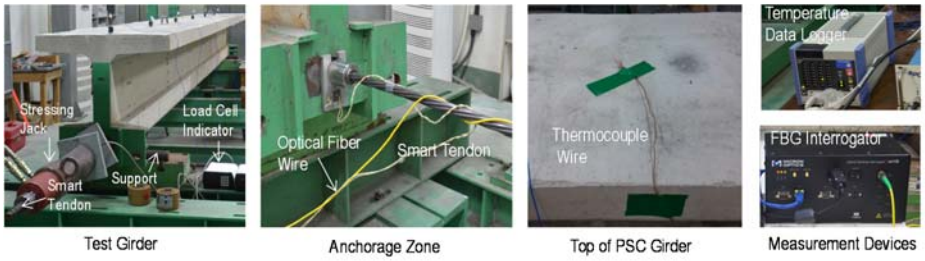

Figure 3.2 Experimental setup in PSCgirder

3.2. Test-Setup of PSC Girder

Lab-scale experiments was conducted on a 6.4-meter PSC girder embedded with a FOS-based smart tendon, as shown in Figure 3.2. The tested T-section girder was simply supported by the steel bars at both ends. The 28-day compressive strength, the elastic modulus, and the mass density the concrete were respectively 23.6 MPa, 24.55 MPa, and 2400 kg/m3. The girder was eccentrically prestressed by a 7-wire straight smart tendon (see Figure 3.1(b)). The eccentricity of the prestress force was 0.324 m from the neutral axis. The prestress forces were introduced into the smart tendon by a stressing jack as the tendon was anchored at one end and pulled out at the other. A load cell was installed at the left end to measure the applied tension force, as shown in Figure 3.2. For temperature monitoring, a K-type thermocouple wire was setup on the top surface of the PSC girder during tests. The unbonded tendon was first pre-tensioned to 138.3 kN (14.1 ton) for the intact state. The reflected wavelengths of the FBG strain sensors were measured by using an optical sensing Interrogator (sm130), as illustrated in Figure 3.2. A KYOWA (EDX-100A) data logger was used to monitor temperature via the K-type thermocouple wire, as shown in Figure 3.2. The 1 Hz sampling rate was set for both the FBG sensing system and the temperature measurement system during the tests.

3.3. Simulations of Prestress-Loss and Temperature Variation

3.3.1. Simulation of prestress-loss

As the first test scenario, the room temperature was controlled by air conditioners in the underground laboratory.

While the laboratory temperature was handled to almost constant of 11ºC, a set of prestress-loss scenarios was simulated to the PSC girder from which the FBG responses of the smart tendon were measured to estimate the tendon force-loss. Fifteen prestressing levels ranging from 138.3 kN to 0 with an interval of approximate 9.81 kN were set for the test structure. By each prestressing levels, four sets of FBG data were sampled. Totally, 60 sets of FOS data were acquired from the FBG sensors. Figure 3.3(a) shows the time history of the measured temperature during the test period on 19 January, 2015. As observed from the figure, the temperature variation was very small, less than 1ºC during the experimental tests.

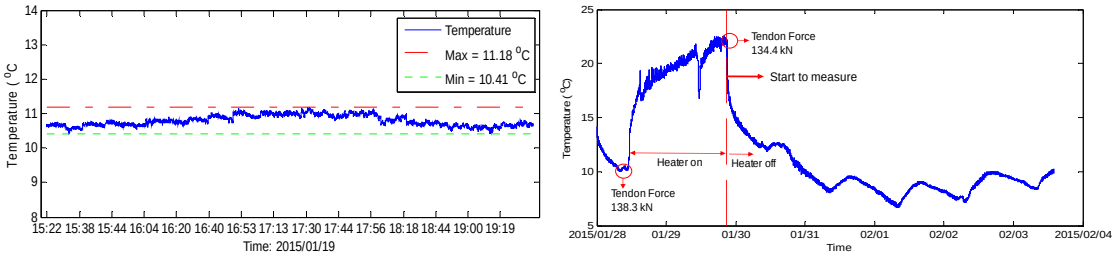

(a) Simulation of unchanged temperature (b) Simulation of temperature variation

Figure 3.3 Time history of temperature scenarios simulated in laboratory

3.3.2. Simulation of temperature variation

As the second test scenario, the laboratory temperature was controlled to vary between 6.6ºC to 22.1ºC while the tension force of the smart tendon was set fixed as 138.3 kN. A series of tests were performed for 7 consecutive days from 28 January to 04 February, 2015 including 2 days for heating and 5 days for auto-monitoring. The time history of the temperature variation simulated in the laboratory is shown in Figure 3.3(b). At the beginning, the heaters were turn on to heat the laboratory temperature up as designed. In the heating process, the tendon forces observed by the load cell were 138.3 kN and 134.4 kN for temperatures of 10ºC and 22.1ºC, respectively. The FOS sensing tests started at 21:00 hour of January 29, 2015 as the laboratory temperature reached up to 22.1ºC. Then the room temperature was controlled to decrease gradually by turning off the heaters for the remaining 5 days. It is noted that the room temperature changed day and night, as shown in Figure 3.3(b).

4. FOS-BASED PRESTRESS FORCE MONITORING AND TEMPERATURE-EFFECT ESTIMATION IN PSC GIRDER

4.1. FOS-based Prestress Force Measurement under Constant Temperature

The prestress-loss in the PSC girder was estimated under the constant temperature. The FOS responses were monitored from the smart tendon for the fifteen prestress force levels ranging from 138.3 kN to 0 kN (i.e., T1 ~ T15). The measured reflected wavelengths of the three FBG sensors (i.e., FBG 1, FBG 2, and FBG 3) are shown in Figure 4.1(a). As observed from the figure, the reflected wavelengths were gradually shifted due to the prestress-loss events. The FOS strains of the smart tendon were then computed using the measured FOS wavelengths for the estimation of prestress-loss, as shown in Figure 4.1(b). As shown in the figure, all three FBG strain sensors embedded in the smart tendon successfully detected the variation of applied prestress forces. Among the three FBG sensors, FBG 3 indicates smaller strain values than those of FBG 1 and FBG 2. It is worth noting that the FBG 3's location is relatively far from the prestressing source (i.e., the prestressing jack), while FBG 2 and FBG 1 were, respectively, located at the middle and the left end of the tendon, as shown in Figure 3.1(b). This indicates that the strain distribution on the smart tendon at each applied load was not uniform, as observed by other researchers (Kim et al. 2011). The relationships between the change of FOS strain responses and the applied tendon force-loss is shown in Figure 4.2(a). It is observed that the FOS strain of the smart tendon varied linearly with the applied tendon force.

From the measured FBG strain, the tension force-loss of the embedded smart tendon was estimated as shown in Figure 4.2(b). As observed from the figure, the prestress-loss estimations by the three FBG sensors were consistently matched with the 45º line. This means, the three FBG sensors well estimated the tension-loss of the unbonded tendon. Relative to FBG 1 and FBG 2, FBG 3 shows smaller errors than the others for the tension-loss prediction. These experimental results have proved the feasibility of the smart tendon as a reliable tension indicator for the PSC girders.

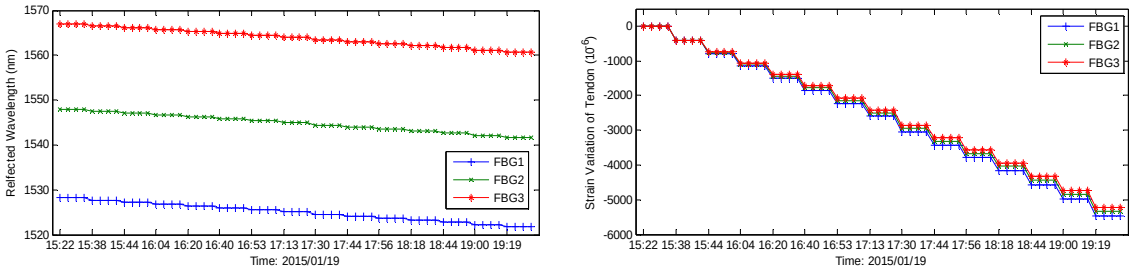

(a) Reflected wavelength (b) FBG strain

Figure 4.1 Time history of reflected wavelength and FBG strain under constant temperature

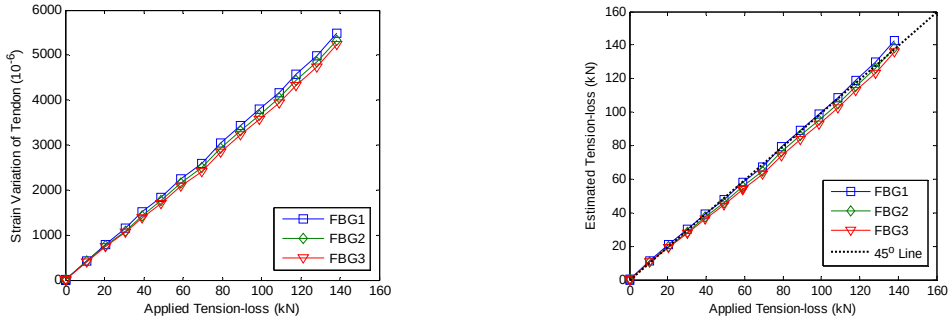

(a) FBG strain vs applied prestress-loss (b) Prestress-loss vs applied prestress-loss

Figure 4.2 Estimation of prestress-loss by FBG sensors under constant temperature

4.2. FOS-based Measurement of Temperature Effect on Prestress Force

4.2.1. Temperature-effect on FOS strain of smart tendon

First, the reflected wavelengths were measured from the FBG sensors embedded smart tendon during the five-day measurement. Then, the FOS strains of the smart tendon were computed from the measured reflected wavelengths. Figure 4.3 illustrates the time history of the smart tendon's thermal strain calculated for the temperatures 6.6 ºC ~ 16.5 ºC by using the FOS response at 16.5 ºC as the reference. Note that the measured FOS data corresponding to the rapid change of temperature (i.e., temperatures 16.5 ºC ~ 22.1ºC) were removed from the analysis since the smart tendon was not sensitive to the quick change of temperature. The thermal strains of the smart tendon are found to change along with the room temperature, but with slight left shifts, as shown in Figure 4.3. This indicates that the embedded tendon of the PSC girder responses more slowly than the surrounding temperature. It is found that the thermal strains of the unbonded tendon increase as temperature increases.

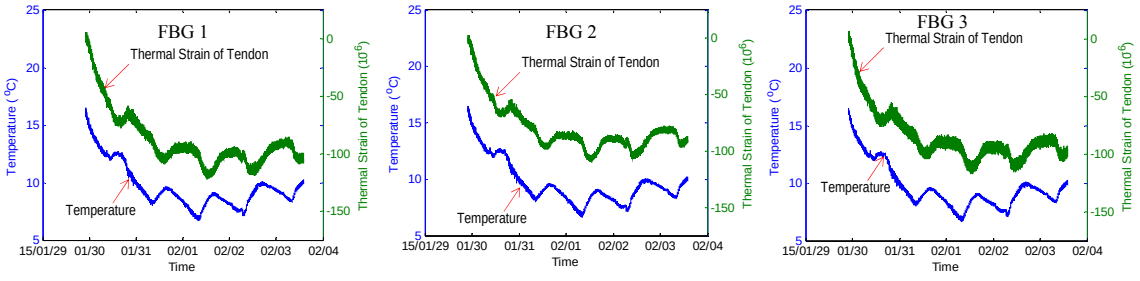

Figure 4.3 Time history of thermal strains of smart tendon under temperature variation

4.2.2. FOS-based measurement of prestress force change due to temperature variation

Next, the prestress force change of the smart tendon was estimated by using its thermal strain responses according to Eq. (2.4). Figure 4.4 shows the time history of the tendon force variation due to the thermal effect calculated for temperatures 6.6 ºC ~ 16.5 ºC. The prestress force and the temperature vary in an opposite manner, as observed in Figure 4.4. The linear regression between the tendon force change and the temperature variation

was analyzed for the three FBG sensors, as illustrated in Figure 4.5. The empirical equations of the tendon force change as a function of temperature are also plotted in Figure 4.5. From the regression analysis, as the temperature increases about 1°C, the prestress-loss predicted by FBG 1, FBG 2, and FBG 3 are, respectively, 0.294 kN, 0.256 kN, and 0.260 kN. The tendon force change due to the temperature effect estimated by the three FBG sensors was compared to the observation by load cell, as shown in Figure 4.6. Remind that the tendon force-loss measured by load cell is about 0.324 kN when the temperature increases about 1°C. It is found that the temperature-effect estimations by the three FBG sensors were well-matched with the indications of the load cell. Among the three FBG sensors, FBG 3 shows the most consistent change in the prestress force under the variation of room temperature.

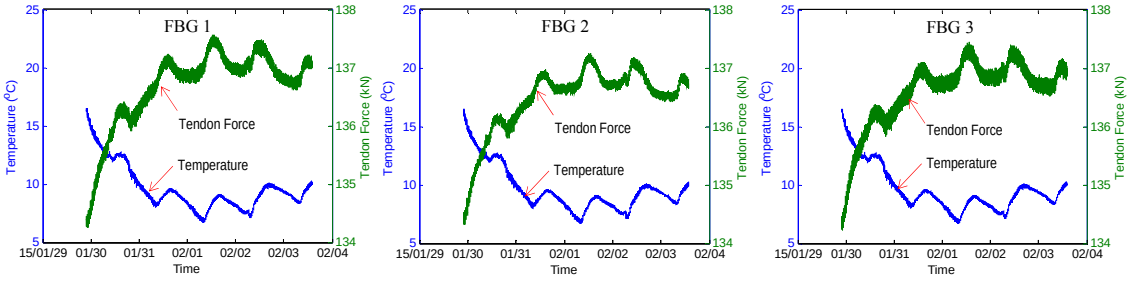

Figure 4.4 Time history of tendon force under temperature variation

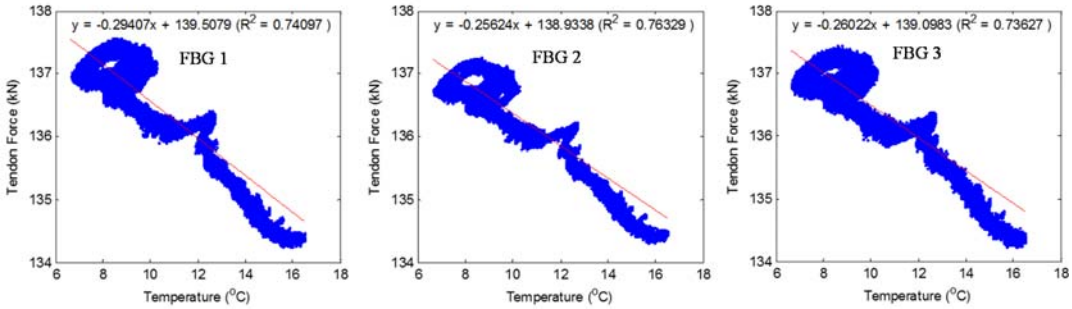

Figure 4.5 Linear regression analysis for tendon force under temperature variation

4.3. Analytical Estimation of Temperature Effect on Prestress Force

By using the known geometries and material parameters described in the previous section, the tensile stiffness of the smart tendon, and the compressive stiffness of the PSC girder were respectively computed as 3.86 MN/m and 31.60 MN/m. Experimental research has shown that the thermal expansion coefficient of the 7-wire prestressing tendon is approximately 14.4×10^{-6} m/m/°C (Chen et al. 2011) and the coefficient of thermal expansion is ranging from 6×10^{-6} m/m/°C to 12×10^{-6} m/m/°C for the concrete girder (Pillai and Menon, 2009). Introducing these values into Eqs. (2.10) and (2.11), the equivalent stiffness k and the longitudinal deformation per Celsius c (m/°C) are computed as 3.75 MN/m, and 18×10^{-6} m/°C ~ 56.4×10^{-6} m/°C, respectively. It is found that the values of c and k are both positive. According to Eq. (2.9), it is predicted that the tendon force change would be negative if temperature increases, and positive if temperature decreases. Figure 4.7 shows temperature-induced tendon force change predicted by 'temperature-effect estimation model' for the various thermal expansion coefficients of the PSC girder. The comparison between the temperature-effect prediction model and the measurement of load cell is also plotted in Figure 4.7. It is found that the prediction model successfully estimated the changing tendency of the tendon force under the temperature variation. It is also observed that the gap between the analytical solution and the measurement of load cell is reduced as the thermal expansion coefficient of the PSC girder decreases.

Temperature-induced variation of tendon forces was compared between the analytical estimation (as shown in Figure 4.7) and the FOS-based measurement (as shown in Figure 4.5). Prediction model corresponding to thermal expansion coefficient 4×10^{-6} m/m/°C of the PSC girder was examined for the comparison, as shown in Figure 4.8. The prediction model analytically estimated the loss of the prestress force by 2.56 kN as temperature was increased by 10°C. Meanwhile, the FOS-based measurements indicated 2.5~3.0 kN as the prestress-loss in

the unbounded tendon of the PSC girder. This prediction is well-matched with the measurements of FBG 2 and FBG 3, and approximate 87% of that of FBG 1.

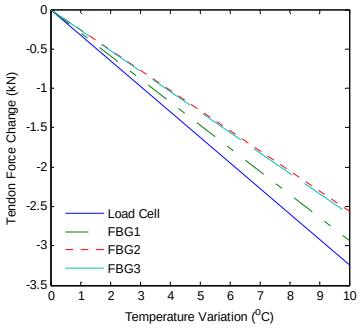

Figure 4.6 Temperature-induced tendon force change measured by FBG sensors and load cell

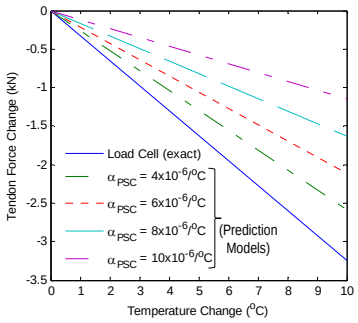

Figure 4.7 Tendon force change predicted by 'temperature-effect estimation model'

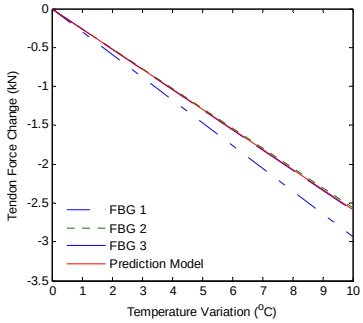

Figure 4.8 Prediction model (α_{PSC} = 4x10^{-6} m/m/°C) versus FOS-based measurement

5. CONCLUSION

From the experimental and analytical analyses, the following conclusions have been made: Firstly, the FBG-sensor embedded tendon successfully monitored the prestress force of the PSC girder. The temperature-driven effect on the prestress force change of the PSC girder was successfully estimated by the FBG sensors embedded smart tendon. Secondly, the prestress force and temperature vary in an opposite manner for the PSC girder – the prestressing tendon is relaxed by losing its tension as temperature increases, and tightened by gaining tension as temperature decreases. Also, the distribution of the thermal strain on the smart tendon was not uniform. Thirdly, the prediction model successfully estimated the changing tendency of temperature-induced tendon force variation in the PSC girder. The temperature effect on the prestress force could be analytically predicted if the thermal expansion coefficient of the PSC girder was well-modeled in the prediction model.

ACKNOWLEDGEMENT

This work was supported by Basic Science Research Program through the National Research Foundation of Korea (NRF) funded by the Ministry of Education, Science and Technology (NFR-2013R1A1A2A10012040). Graduate students involved in this research were also supported by the Brain Korea 21 Plus program of Korean Government.

REFERENCES

1. Adams R.D., Cawley P, Pye C.J., Stone B.J. (1978), "A Vibration Technique For Non-Destructively Assessing The Integrity Of Structures", *Journal of Mechanical Engineering Science*, **20**, 93-100.
2. Hong, D.S., Park, J.H., Kim, J.T., and Na, W.B. (2009), "Temperature Effect on Hybrid Damage Monitoring of PSC Girder Bridges by Using Acceleration and Impedance Signatures", *SPIE*, **7292**,CA.
3. Kim, Y.S., Sung, H.J., Kim, H.W., and Kim, J.M. (2011), "Monitoring of Tension Force and Load Transfer of Ground Anchor by Using Optical FBG Sensors Embedded Tendon", *Smart Struct. Syst.*, **7:4**, 303-317.
4. Miyamoto A., Tei K., Nakamura H., Bull J.W. (2000), "Behavior of Prestressed Beam Strengthened with External Tendons", *Journal of Structural Engineering*, **126:9**, 1033-1044.
5. Ni, Y.Q., Hua, X.G., Fan, K.Q., and Ko, J.M. (2005), "Correlating Modal Properties with Temperature Using Long-Term Monitoring Data and Support Vector Machine Technique", *J. of Eng. Struct.*, **27**, 1762-1773.
6. Othonos, A. andKalli, K. (1999), Fiber Bragg Gratings, Artech House, London.
7. Pillai, S. and Menon, D. (2009), "Reinforced Concrete Design - Third Edition", *Tata McGraw-Hill Education Private Limited*.
8. Saiidi, M., Douglas, B. and Feng, S. (1994), "Prestress Force Effect on Vibration Frequency of Concrete Bridges", *J. Struct. Eng., ASCE*, **120:7**, 2233-2241.
9. Stubbs N., Osegueda R. (1990), "Global non-destructive damage evaluation in solids", The International *Journal of Analytical and Experimental Modal Analysis*, **5:2**, 67-79.